Organic dyads and triads based on the triphenylene-rylenediimide couple: Molecular design, self-organization, and photo-physical properties

Hang Lin, Qiu-Bing Lv, Hai-Feng Wang, Ke-Qing Zhao, Ping Hu, Bi-Qin Wang, Benoît Heinrich, Bertrand Donnio

Organic dyads and triads based on the triphenylene-rylenediimide couple: Molecular design, self-organization, and photo-physical properties

Hang Lin,[a] Qiu-Bing Lv,[a] Hai-Feng Wang,[a] Ke-Qing Zhao,[a,*] Ping Hu a,[a] Bi-Qin Wang,[a] Benoît Heinrich,[b] Bertrand Donnio,[b,*]

[a] College of Chemistry and Material Science, Sichuan Normal University, Chengdu, 610066, China ; E-mail address: kqzhao@sicnu.edu.cn (K.-Q. Zhao).

[b] Institut de Physique et Chimie des Mat´eriaux de Strasbourg (IPCMS), CNRS-Université de Strasbourg (UMR 7504), 67034, Strasbourg Cedex 2, France ; E-mail address: bdonnio@ipcms.unistra.fr (B. Donnio).

Dyes Pigm. **2022**, *197*, 109911. DOI: 10.1016/j.dyepig.2021.109911

Received: 8 July 2021; Revised14 September 2022; Accepted 22 October 2021

Published: 28 October 2021

Keywords: Molecular heterojunction, Discotic liquid crystal, Triphenylene, Perylene bisimide, Benzoperylenebisimide, Hexagonal/rectangular columnar phase, Photoluminescence, Electron donor/acceptor, Photo-induced electron/energy transfer, Density function theory calculation, Orbital frontiers

Highlights

- Dyad and triad discotic mesogens were synthesized by Sonogashira coupling/DBU-promoted cyclization reactions tandem.
- Fluorescence quenching is observed for all compounds due to photo-induced electron transfer between donors and acceptors.
- The compounds exhibit hexagonal and rectangular columnar mesophases over broad temperature ranges.

Abstract

Liquid-crystalline D-A dyads and A-D-A triads, based on the chemical association of electron-donor (D) triphenylene discogens and electron-acceptor (A) perylene/benzoperylene diimides, have been synthesized by the Pd-catalyzed Sonogashira coupling/DBU-promoted cyclization reactions tandem. These molecular heterojunctions spontaneously self-organize into columnar hexagonal

(Col_{hex}) or/and rectangular (Col_{rec}) mesophases, over broad temperature ranges including room temperature, with the antagonist moieties segregated into alternated homo-molecular (homolithic) stacks within mixed columns. Their intramolecular electron and energy transfers have been studied by UV/Vis absorption and fluorescence emission spectroscopies. Due to photo-induced electron transfer between donor and acceptor units, fluorescence quenching is systematically observed for all the dyads and triads. This study further reveals that perylenediimide is a stronger electron acceptor than the larger benzoperylenediimide building block. Density function theory calculations of their molecular structures and HOMO-LUMO energy levels and gaps support the experimental results and demonstrate that these donor-acceptor systems have potential applications in various optoelectronic devices.

1. Introduction

In many organic-based optoelectronic devices, such as photovoltaic solar cells (PSCs) and light emitting diodes (OLEDs), the active materials usually consist of electron-donor and acceptor molecules (for PSCs), and electron- or hole-transporter moieties (for OLEDs) [1]. Such types of molecular materials could play an essential role in future organic electronic devices, as, for instance, ambipolar semiconductors [2]. According to the devices' structure and active materials, organic solar cells can be categorized into bilayer solar cells, bulk heterojunction solar cells, and molecular heterojunction solar cells [3]. Of interest are the molecular heterojunctions, which consist of chemically linked electron-donor (D)/-acceptor (A) moieties via alkyl spacers, as the ideal device configuration for the photoinduced energy and charge transfer, and for the charge collection and transport in organic photovoltaic solar cells [4], [5], [6]. When an active layer is made of such molecular heterojunctions, one has to ensure that both A and D entities phase separate at the nanometre scale, with ideally, the largest D/A interface [4],[5]. If nanoscale segregation is realized by molecular self-sorting, molecular heterojunctions should be promising supramolecular structures for these applications. Although, as evidenced by the numerous reported attempts in the literature, these molecular heterojunctions do not seem straightforward to design since both entities tend to neutralize each other by mixing rather than by segregating, and their design still remains a timely challenge [4].

π-Conjugated discotic liquid crystals (πDLCs) made of large polycyclic aromatic cores [7], [8], [9] are among the most attractive materials in organic electronics as organic semiconductors. Indeed, πDLCs are outstanding examples of soft self-assemblies: they self-organize with self-healing ability into columnar phases with a large degree of stacking order, and show extraordinary unidirectional charge migration properties [10], [11], [12], [13], [14], [15]. They have potential applications for uses in optoelectronic devices, such as organic field-effect transistors (OFETs) [16], OLEDs [17], [18], [19], or OPSCs [1].

On the one hand, electron-rich triphenylene derivatives (**TP**) are being widely studied as p-type semiconducting DLCs (for positive charge hopping pathway) because of their natural tendency to stack into columns and to self-assemble into columnar mesophases [20], [21], [22]. On the other hand, electron-deficient perylene bisimides (**PI**) and related rylene derivatives [23],[24] are among the best n-type organic semiconductors (for electron transport), in replacement of fullerene (C_{60}) derivatives [23],[24], but have however been less investigated as discotic liquid crystals essentially due to their low solubility in organic solvents [25], [26], [27]. Introduction of long alkyl groups at either both imide tips or at the *ortho*/*bay* positions of the **PI** cores has

improved drastically their solubility as well as significantly promoted self-assembly in liquid crystal mesophases.

As just mentioned above, and essentially for molecular design considerations, only a few examples of such D–A mesomorphic molecular architectures, mainly triphenylene-rylene molecular heterojunctions, where the n- and p-type entities truly separate in space, have been reported so far [28], [29], [30], [31], [32], [33], [34], [35]. The search for other multi-segregated supramolecular self-assemblies is still essential and therefore highly desirable for the design of efficient ambipolar systems.

Previously, we obtained D-A-D molecules associating triphenylenes and rylenes, in which both electron-donating and accepting species were found to self-segregate into lamello-columnar (LamCol) mesophases, as demonstrated by small-angle X-ray diffraction and STM studies, thus forming distinct electron and hole transport pathways, and showing high electron and hole mobility values [35]. Here, we report on the synthesis, thermal and self-assembly behaviours, and optical properties of triphenylene-rylenebisimide donor-acceptor (D-A) dyads and A-D-A triads, with the inverted topology as previously reported [35]. Thermal gravimetry (TGA), polarizing optical microscopy (POM), differential scanning calorimetry (DSC), and small- and wide-angle X-ray scattering (S/WAXS) revealed that all compounds are highly thermally stable and that they all self-organize into wide-temperature ranges columnar mesophases, including room temperature, with only local-range segregation of the different moieties within mixed columns. The electron and energy transfers between the donor and acceptor have been studied, revealing that perylenediimide is a stronger electron acceptor than the larger benzoperylenediimide building block, in agreement with Density Function Theory (DFT) calculations of their molecular structures, frontier molecular orbitals and energy gaps.

2. Results and Discussion

2.1. Design, synthesis and characterization

In order to improve the solubility of both the discotic fragments in organic solvents and to promote the formation of low-transition temperatures columnar mesophases (including room temperature) with **TP**-**PI** dyad and **TP**-**PI2** triad (and their benzoperylenediimide homologs, **BP**), two bulky forked chain fragments were grafted on either tip of the **PI** core, whilst the **TP** periphery was decorated by 5 and 4 octyloxy chains, for the dyads and triads, respectively. A flexible spacer, connecting the **TP** entity at one or two of the vacant position(s) with one of the *bay* positions of the **PI** unit, was set sufficiently long to allow their spatial separation. The perylene-containing compounds (**TP**-**PI** and **TP**-**PI2**, Scheme 1) were synthesized in one step by palladium-catalyzed Sonogashira cross-coupling reaction between bromoperylene bisimide and mono- or di-alkynyl triphenylene precursors, respectively (**PI**–**Br**, **TP**-**1** and **TP**-**2**, Scheme 1) in 50–55% yields. Subjecting **TP**-**PI** and **TP**-**PI2** to the strong base diazabicyclo[5.4.0]undec-7-ene (DBU), promoted intramolecular cyclization, leading to the corresponding benzoperylene derivatives (**TP**-**BP** and **TP**-**BP2**, Scheme 1) in 70 and 55% yields, respectively.

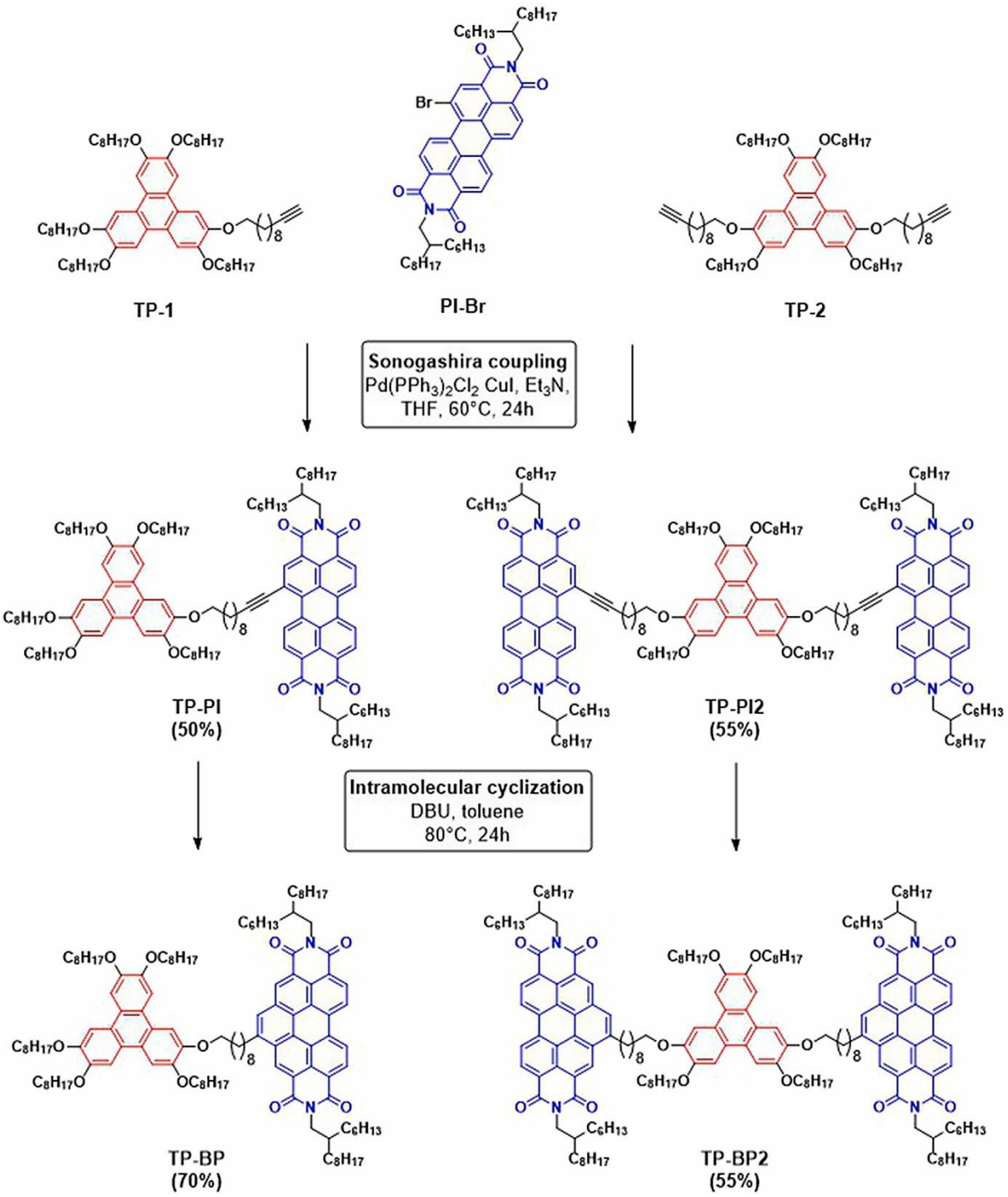

Scheme 1. General synthetic scheme, molecular structures, yields and nomenclature of electron donor-acceptor (D–A) dyads (**TP**-**PI**, **TP**-**BP**) and A-D-A triads (**TP**-**PI2**, **TP**-**BP2**).

The branched chain perylene bisimide **PI** was synthesized in high yield (85%) using a classical procedure (Supplementary Information, Scheme S1). Bromation of **PI** performed with 1 equivalent of bromine yielded, after purification by chromatography, the isomerically pure compound, **PI**-**Br**, in 43% yield. Both the mono- and di-alkynyl triphenylene discogens, **TP**-**1** and **TP**-**2**, were synthesized by the Williamson ether reaction between 2-hydroxy-3,6,7,10,11-

pentakis(octyloxy)triphenylene and 2,7-dihydroxy-3,6,10,11-tetrakis(octyloxy)triphenylene [36], respectively (Scheme S2), and 10-undecyn-1-yl *p*-toluenesulfonate (Scheme S3).

The intermediates were characterized by ^{1}H NMR and all the final target molecules were characterized by ^{1}H NMR, ^{13}C NMR, HRMS and elemental analysis (see Supplementary Information, Figures. S1–S23). The results revealed the good purity of the compounds and the good agreement with the expected molecular structures.

2.2. Thermal stability, mesomorphism, supramolecular organization

As expected, this specific molecular design promotes the self-organization of the D-A structures into room-temperature columnar mesophases. The thermal stability and mesomorphic behaviour of the D-A and A-D-A compounds were first investigated by POM, TGA and DSC (results summarized in Table S1), prior to the structural characterization of the mesophases by S/WAXS. The excellent thermal stability of the dyads and triads was confirmed by thermal gravimetric analysis (TGA in dynamic mode, Figure 1). Indeed, in all 4 cases, the decomposition temperatures (considered at the onset of the 5% weight loss) are all remarkably higher than 350 °C. Accordingly, no sign of decomposition could be detected by POM in the mesomorphous temperature interval, even in the isotropic state, and the transition temperatures were fully reproducible on subsequent heating-cooling cycles.

As evidenced by POM, the four target compounds revealed fluid and birefringent textures (Figure 1) typical of liquid crystalline mesophases, but not characteristic, from room temperature onwards. These observations thus did not permit their unequivocal assignment, except for **TP**-**PI**, whose texture exhibits in addition large homeotropic zones, corresponding to columns of stacked molecules oriented perpendicular to the untreated glass substrates, a good indication of the formation of a columnar hexagonal phase (Col_{hex}). No structural change could be observed on further heat-cool cycles, suggesting the presence of one single mesophase per compound only, as also confirmed by DSC analysis (Figure 1); crystallization was not observed for any of them up to below −50 °C. Both the dyads **TP**-**PI** and **TP**-**BP** exhibit a similar thermal behaviour with only one endotherm detected by DSC, corresponding to the clearing temperature, at ca. 130 and 141 °C on heating, respectively (Table S1). These transition temperatures are perfectly reversible on cooling, with almost no delay in the mesophase reformation (Table S1). The triads **TP**-**PI2** and **TP**-**BP2** also displayed only one endotherm, with higher isotropization temperatures than their corresponding dyads. A substantial increase of the mesophase stability was found for the **BP**-containing triad with respect to the **PI** triad, from 181 and up to 230 °C on heating, respectively.

As already previously noted with other structurally related alkyne-containing compounds [35], **TP**-**PI2** exhibited partially heating-induced polymerization above 200 °C if maintained at this temperature for prolonged periods of time, and with evidences of irreversible thermal behaviour after repeated DSC heat-cool treatments and the observation of small domain-formation in POM texture.

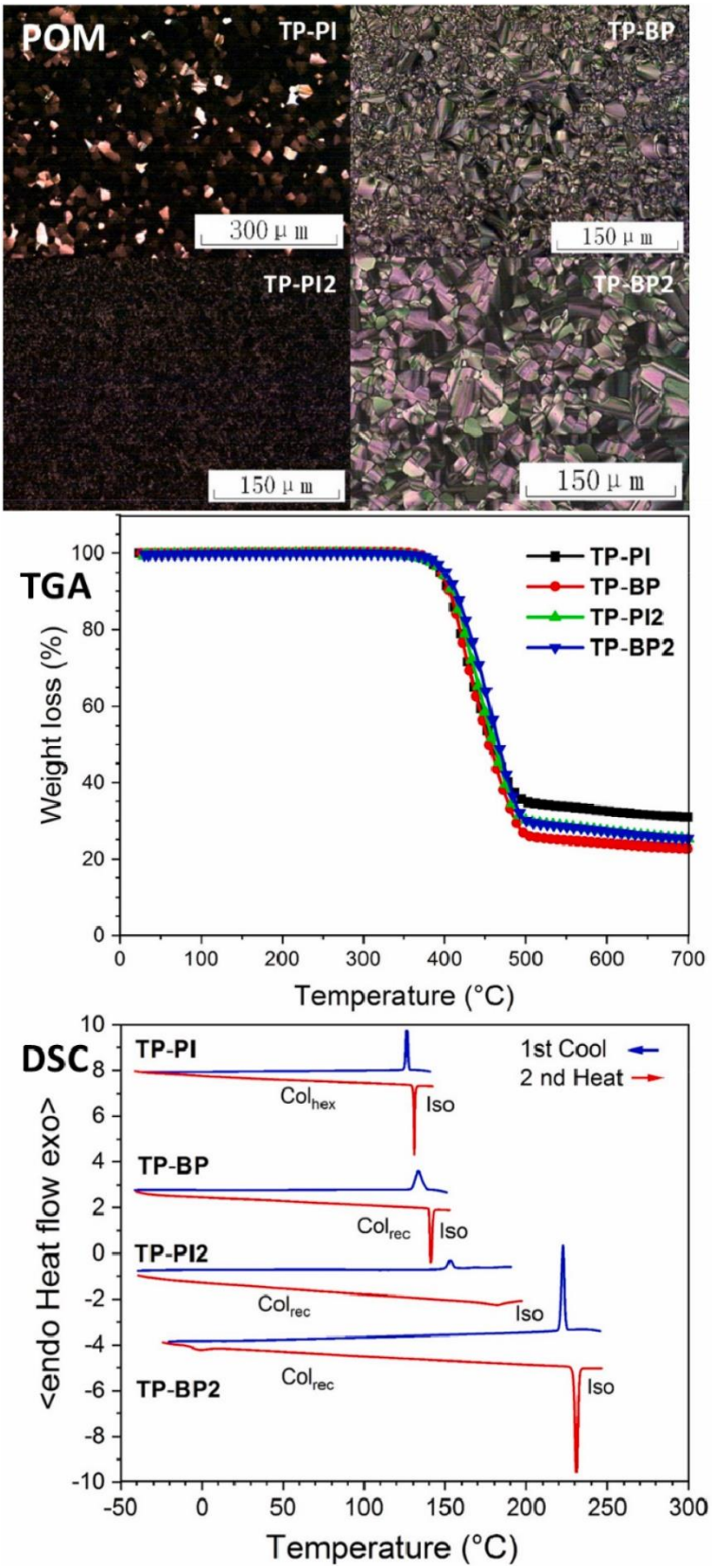

Figure 1. Representative optical photomicrographies (POM, on cooling from the isotropic liquid) of the D-A dyads and A-D-A triads in the mesophases: **TP-PI** at 115 °C in Col_{hex}, **TP-BP** at 126 °C in Col_{rec}, **TP-PI2** at 153 °C in Col_{rec}, **TP-BP2** at 230 °C in Col_{rec}. Thermal gravimetry curves (TGA, dynamic mode), heating rate 10 °C min^{-1}, under N_2; the 5% weight loss temperatures were 402, 395, 397 and 395 °C for **TP-PI**, **TP-BP**, **TP-PI2**, and **TP-BP2**,

respectively. Differential scanning calorimetry (DSC) traces at scanning rate of 10 °C min^{-1}, first cooling (blue curves), and second heating (red curves). (For interpretation of the references to colour in this figure legend, the reader is referred to the Web version of this article.)

Thus, the triads show higher phase transition temperatures and mesophase stability than the dyads, as well as the **BP** derivatives with respect to the **PI** systems. This tendency can be understood by the enhancement of π-π interactions upon the change of the molecular structures and the increase conjugation (dyads→triads:+50,+90 °C, **PI**→**BP**:+10,+50), hence stronger packing cohesion in columns, and therefore the increase of the thermal stability and phase transition temperatures. Furthermore, mesomorphism was strongly promoted by chemically connecting both types of molecular species. As far as the precursory fragments are concerned indeed, only the mono-functional discogen **TP**-**1** was mesomorphous, exhibiting a Col_{hex} mesophase with a narrow, though low, temperature range (Cr 50 Col_{hex} ~ 61 Iso/Iso 58 Col_{hex} ~ 28), whereas both the di-functional **TP**-**2** (Cr 61 Iso/Iso 33 Cr) and **PI**-**Br** (Cr 132–134 Iso) melted directly in the isotropic liquid without showing any mesophase (Figures S24–S25).

The mesophases' structures were investigated by S/WAXS and the representative X-ray patterns of **TP**-**PI**, **TP**-**BP**, **TP**-**PI2** and **TP**-**BP2**, recorded on cooling from the isotropic liquid at room temperature are shown in Figure 2a, and the structural and geometrical data are reported in Table 1. The assignment to *p*6*mm* Col_{hex} mesophase for **TP**-**PI** suggested by POM was confirmed by the presence of only one single sharp and intense small-angle reflection, indexed as (10). In the wide-angle range, two additional signals were observed: i) the intense semi-diffuse peak, at around 3.5 Å, arising from the regular distance between triphenylene or perylene rings, respectively, piled into columns ($h_{TP} \approx h_{PI} \approx h\pi$, *a priori* undifferentiated), with a correlation length, ξ ≈ 40 Å, corresponding to molecular stacks of ca. 11 mesogens, and ii) the strong and broad scattering with a maximum in the 4.5–5.0 Å range, due to liquid-like lateral distances between molten chains (h_{ch}). Due to the sole presence of the intense small-angle reflection (10), a square symmetry could also have been suggested, but this possibility was disregarded as incompatible with the dimensions of the dimer, too large to be accommodated within the lattice without a significant tilt with respect to the symmetry plane (For a Col_{squ} at T = 25 °C, a_{squ} = 18.78 Å, Z = 1, γ = 90°, A_{squ} = 352.8 $Å^2$, h_{mol} = 4.27 Å, ψ ≈ 35–40°).

The S/WAXS patterns of the other 3 compounds showed two intense diffraction peaks in the small-angle region, indexed as the fundamental reflections (20) and (11) of a rectangular lattice, plus additional very weak diffraction peaks corresponding to the (31) and (02) indexations (Table S2). Similarly, the semi-diffuse peak at ca. 3.5 Å (ξ ≈ 30-55 Å, ca. stacks of ca. 9–16 mesogens on average) and the broad scattering at ca. 4.5 Å correspond, as above, to the stacking of the **TP**, **PI**/**BP** aromatic cores and to the average lateral distances between molten chains, respectively. The mesophase is the same for the three compounds and could be safely assigned to as rectangular columnar mesophase (Col_{rec}) with the *c*2*mm* planar symmetry.

The major changes in mesophases' structural parameters consist in the larger lattice elongation in the triad architecture, imposed by the larger proportion of the non-symmetrical rylene mesogens (**PI** and **BP**) and to the loss of the preferential orientation in the particular case of the **TP**-**PI** dyad (whose lattice parameters hardly change with temperature). In the Col_{hex} phase, the lath-shaped **PI** have no preferential orientation likely due to mismatch of chains' substitution patterns (Figure 2c) leading to overall

circular columns, whilst in the Col_{rec} phase of **TP**-**BP**, **TP**-**PI2** and **TP**-**BP2**, the rylene cores align preferentially along defined directions (along the a-lattice axis), causing the elongation doubling and the symmetry breaking of the lattice to rectangular symmetry *c*2*mm* (solid line frames, Figure 2b). The elongation markedly increases with temperature, which is the logical consequence of the lower degree of stretching of the alkyl spacers connecting column walls. The lattice area on the contrary just follows the normal volume expansion with temperature, resulting in quite constant molecular slice thicknesses (h_{mol} = 3.52–3.85 Å, Table 1, obtained as the ratio between half a dyad or a third of a triad volume with the average cross-section of one column, A/Z). These average values are slightly, but significantly, above the face-to-face stacking distances directly determined from wide-angle scattering maxima (h_π), which might either come from slightly out-of-plane tilted mesogens (by 18 ± 5°, ψ, Table 1) and/or from orientational fluctuations.

The detailed analysis of the mesophases' geometrical parameters (lattices' parameters and areas, Table 1) reveals that both the Col_{hex} (**TP**-**PI**) and Col_{rec} (**TP**-**PI2**, **TP**-**BP**, **TP**-**BP2**) phases are therefore constituted of one single (Col_{hex}) and two (Col_{rec}) columns per lattice, respectively, composed of *a priori* undifferentiated triphenylene/rylene mesogenic stacks, thus ruling out the formation of multicolumnar superlattices [30]. This implies that both mesogens somehow periodically distribute along the columns.

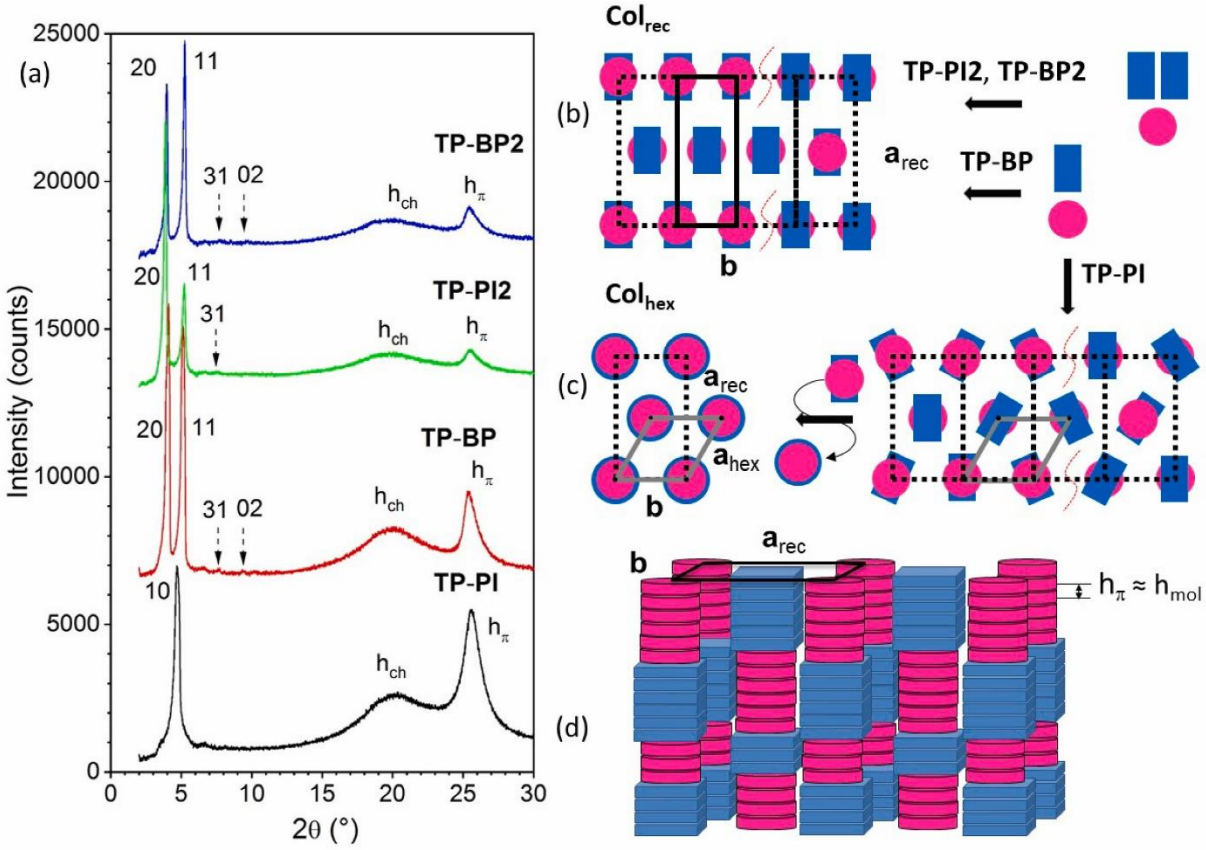

Figure 2. (a) Representative S/WAXS patterns of dyads/triads at room temperature (and 70 °C for **TP**-**PI2**). (b,c) Symmetries and geometrical local-range representations of the columnar arrangements exhibited (b, Col_{rec}; c, Col_{hex}) by dyads and triads combining triphenylene (**TP**, pink discs) and side-attached rylene (**PI** or **BP**, blue rectangles). Solid frame: hexagonal (grey)

and rectangular (black) lattices; dotted frame (see text). (d) Schematic representation of the supramolecular arrangement in domains of the various columnar phases: for the Col_{rec} phase, **TP** and **PI**/**BP** columnar homo-molecular stacks alternate while preserving the orientation of the **PI**/**BP** stacks; for the Col_{hex} phase, the blue tiles (**PI**/**BP**) are freely orientated to yield time-averaged discoid shape (not represented). The dashed red curves represent the permutation of the columnar domains. (For interpretation of the references to colour in this figure legend, the reader is referred to the Web version of this article.)

Therefore, this simple molecular design did not permit, as demonstrated by the non-formation of superlattices (S/WAXS), to obtain the desired so-called “double-cable” mesophases, consisting of separate columns purely made of **TP** units alternating with columns solely constituted of **PI**/**BP** species, an essential condition for the fabrication of OPV devices. *A contrario*, the columns of both Col_{hex} and Col_{rec} phases appear undifferentiated at the macroscopic level, with the apparent homogeneous mixing of **TP** and rylenes along the columns (i.e. complete loss of differentiation between **TP** and **PI**/**BP** fragments). Despite that individual mesogenic rylene diimides and triphenylenes self-organize into columnar stacks with rather similar stacking distances ($h_{\mathbf{TP}} \approx h_{\mathbf{PI/BP}} \approx h_{\pi}$) [21],[26], their intrinsic chemical nature, shape and the symmetry of the chains' substitution pattern (here, **TP** has C_3-type chains’ pattern, and **PI**, a C_2-type) are substantially different rendering their complete intimate mixing by CT interactions in single mixed stacks highly doubtful. Indeed, such a homogeneous stacking of **TP** and **PI** (**BP**) units would likely cause thermodynamically-unfavorable interactions between alkyl chains of the **TP** mesogens and the core of the **PI** units, and would foster their self-sorting assembly into uniform and distinct homolithic columns [37]. In order to support the hypothesis of mixed columns of alternating blocks, DSC experiments (supported by POM) were performed on 1:1 and 1:2 M mixtures of their single components **TP-1** and **TP-2** with **PI** and **BP** model compounds, respectively. It was found that overall these compounds phase segregate and still behave almost as individual components (Figure S26) [38]. Hence, the supramolecular arrangement of the dyads and triads must be somehow a compromise between both extreme situations i.e. uniform A-B-A-B … intimate mixing in one single column *versus* complete phase separation into two distinct segregated columns (A-A-A … or B–B–B …). It is proposed based on the above arguments that the various molecules self-assemble into some kind of mixed D/A columns, made of the alternation of short-range homolithic D- or A-stacks. The apparent loss of differentiation at the molecular scale is most likely consequent to the periodic permutation of entire groups of identical mesogens, within stacks of mesogens, with an average of about 10–15 identical mesogens per stack (Figure 2d) and at larger scale between neighboring columnar domains. These permutations would be facilitated by the partial erasing of the shape differences between the two types of mesogens by the lateral chains of the **TP** compounds on the one hand, and the long aliphatic spacers and the bulky ramified chains at the rylene tips, on the other hand.

Table 1. Structural and geometrical parameters of the dyads and triads mesophases, at various temperatures.

Cpds	T[a]	Phase [b]	V_{mol}[c]	ρ[c]	χ_{ch}[d]	n_{mes}[e]	a[f]	b[f]	A[Z][f]	$a/b\sqrt{3}$[f]	h_{mol}[g]	h_{π} (ξ)[h]	ψ[i]	A_{core}[j]	D_{cyl}[k]	σ_{cyl}[l]	q[m]
TP-PI	25	**Col_{hex}**	3016	1.03	0.712	2	37.56	21.69	407.2[1]	1	3.70	3.48 (42)	20	117.3	12.22	23.68	1.11
TP-PI	55	**Col_{hex}**	3084	1.00	0.715	2	37.82	21.84	412.9[1]	1	3.73	3.50 (37)	20	117.7	12.24	23.91	1.10
TP-PI	85	**Col_{hex}**	3152	0.99	0.720	2	38.06	21.97	418.2[1]	1	3.77	3.53 (28)	20	117.1	12.21	24.10	1.08
TP-PI	115	**Col_{hex}**	3219	0.97	0.729	2	38.06	21.97	418.2[1]	1	3.85	3.56 (23)	22	113.3	12.01	24.22	1.06
TP-BP	30	**Col_{rec}**	3035	1.02	0.710	2	43.07	18.80	809.7[2]	1.323	3.75	3.49 (57)	21	117.4	12.23	24.00	1.12
TP-BP	60	**Col_{rec}**	3102	1.00	0.714	2	44.45	18.76	833.9[2]	1.368	3.72	3.53	18	119.2	12.32	24.00	1.10
TP-BP	90	**Col_{rec}**	3170	0.98	0.720	2	44.64	18.79	838.8[2]	1.372	3.78	3.54	20	117.4	12.23	24.20	1.08
TP-BP	120	**Col_{rec}**	3238	0.96	0.728	2	44.95	18.92	850.5[2]	1.372	3.81	3.57	20	115.7	12.14	24.21	1.06
TP-PI2	25	**Col_{rec}**	4332	1.05	0.690	3	45.40	18.06	819.9[2]	1.451	3.52	3.44	13	127.0	12.72	23.44	1.10
TP-PI2	70	**Col_{rec}**	4477	1.02	0.696	3	45.60	18.16	828.1[2]	1.450	3.60	3.49 (46)	14	125.9	12.66	23.86	1.08
TP-PI2	115	**Col_{rec}**	4623	0.99	0.707	3	46.36	18.11	839.6[2]	1.478	3.67	3.54	15	122.9	12.51	24.04	1.06
TP-PI2	160	**Col_{rec}**	4768	0.96	0.724	3	47.02	18.14	852.9[2]	1.497	3.73	3.57	15	117.8	12.25	23.92	1.02
TP-BP2	25	**Col_{rec}**	4344	1.05	0.688	3	44.23	18.05	798.4[2]	1.415	3.63	3.48 (55)	15	124.5	12.59	23.93	1.12
TP-BP2	80	**Col_{rec}**	4523	1.01	0.696	3	45.26	18.16	821.9[2]	1.439	3.67	3.51 (48)	17	124.9	12.61	24.24	1.09
TP-BP2	135	**Col_{rec}**	4701	0.97	0.712	3	46.60	18.04	840.7[2]	1.491	3.73	3.54 (40)	18	121.0	12.42	24.25	1.05
TP-BP2	190	**Col_{rec}**	4880	0.94	0.735	3	47.35	17.99	851.8[2]	1.520	3.82	3.60 (30)	19	112.9	12.00	23.99	1.00

[a]Temperature (°C) of experiment; [b]Mesophase type; [c]Molecular volume (Å^3) and density (g.cm^{-3}) calculated by additivity of partial elementary volumes; [d]Aliphatic volume fraction ($\chi_{ch} = V_{ch}/V_{mol}$, $\chi_{core} = 1- \chi_{ch}$; [e]$n_{mes}$: number of mesogens per molecule ($n_{mes} = 2$ for dyads and 3 for triads); [f]Lattice parameters (Å), areas (Å^2) and number of columns (Z) per lattice: i) Col_{hex}: $b = a_{hex}$ ($a = b\sqrt{3}$), $\gamma = 120°$, $A = a_{hex}^2 \sin\gamma$, $Z = 1$ column per lattice; with rectangular coordinates: $b = b_{rec}$, $a = a_{rec} = b\sqrt{3}$, , $\gamma = 90°A = b\times a$, $Z = 2$; ii) Col_{rec}: $a= a_{rec}$, $b = b_{rec}$, $\gamma = 90°A = b\times a$, $Z = 2$; elongation of the columnar lattice in the a-axis (a_{rec}) direction with respect to hexagonal geometry; [g]Columnar slice thickness $h_{mol} = (V_{mol}/n_{mes})/(A/Z)$ in Å; [h]Face-to-face π-π stacking distance (Å) from scattering maximum from S/WAXS pattern, and □, correlation length (Å) determined by Debye-Scherrer formula; [i]Out-of-plane tilt angle (°) of mesogen cores inside columns; [j]Cross-sectional area of columnar cores (Å^2): $A_{core} = (1-\chi_{ch})A/Z$; [k]Diameter (Å) of equivalent circular cross-sectional area A_{core}, $D_{cyl} = \sqrt{(4\times A_{core}/\pi)}$ for **TP** moieties; [l]Cylinder area (Å^2) per chain: $\sigma_{cyl} = \pi D_{cyl}\times h_{mol}/n_{ch}$, where $n_{ch} = 6$ for the dyads and the triads (chains around **TP** part); [m]Chain packing ratio: $q = \sigma_{cyl}/\sigma_{ch}$, σ_{ch} being the cross-sectional area (Å^2) of a molten chain.

From a geometrical point of view, the mesogens can therefore be averaged to pseudo-disc-shaped units of dimensions defined by the columnar section and the average molecular slice thickness, h_{mol} (Table 1). The average area needed by the peripheral chains is perfectly compatible with the interface area offered by the non-tilted stacked mesogens, since the mean ratio q_{cyl} (Table 1) between required and available areas does not deviate from unity [39]; the chains are therefore fully stretched in the plane and densely packed in this case, which suggest that the deficiency of chains around the **PI**/**BP** units is well compensated by the lateral **TP** chains from neighboring columns (Figure 2d). The absence of a three-dimensional order in the mesophases also implies the variation of homolithic stacks periodicity along the columns, but still remains more or less matched (mirrored) with the surrounding neighboring columns (Figure 2d). This compensation process and the chemical connection between both entities likely disturbs the free rotation, even more for the triads, stabilizing the rectangular symmetry more efficiently. The proposed supramolecular model (Figure 2d) is further consistent with the relative mesophase stability (i.e. temperature range) observed in this series of compounds.

Along this line, lamello-columnar mesophases with alternating rows of **TP** and rylene columns were reported for the inverted triads **PI**-**TP2** and **BP**-**TP2**, with short spacers (propyl instead of octyl) and octyl end-chains [35]. The fact that even the lattice elongation vanish for the **TP**-**PI** is understandable by the conjunction of the longer alkyne spacers and of the dyad stoichiometry. This configuration is intrinsically more favourable to permutation of column segments, since only the triad stoichiometry may realize the ideal separation of components at the nodes and centres of honeycomb lattices [30].

2.3. Photophysical properties

Electronic energy transfer and electron transfer are fundamental and ubiquitous mechanisms in chemistry, physics and biology [40], [41], [42], [43]. Understanding intramolecular energy and electron transfers for these electron-donor/acceptor dyads and triads is important for further molecular designs and extending the potential of these mesomorphous materials [42]. Hexa(alkoxy)triphenylene (**TP**) and perylene diimide (**PI**) are both outstanding fluorophores, and the latter exhibits almost 100% fluorescent quantum yield in solution [25].

UV/vis absorption and photoluminescent spectra (Figures 3-4, S28-S29) of the dyads and triads were recorded in dilute solutions (1×10^{-6} M in CH_2Cl_2) and compared to reference compounds **PI**, **BP** and **TP**-**1** (the structures of the latter ones are shown in Figure S27). **TP**-**PI**/**TP**-**PI2** show similar UV/vis absorption bands with absorption of **TP** core and **PI** core peaking at 278, 500, and 538 nm, respectively (Figure 3a). The visible absorption bands of **TP**-**BP**/**TP**-**BP2** are blue-shifted by about 63 nm compared to the **TP**-**PI**/**TP**-**PI2** pair, due to the change of their aromatic π-conjugation. The A-D-A triads show similar absorption behaviour to the corresponding D-A dyads except that they display stronger bands due to the two acceptors per molecule and more broadened spectra due to the stronger aggregation behaviour. The slight red-shift of **TP**-**PI**/**PI2** compared to the pure reference compound **PI** is likely caused by the π-conjugation extension of the alkynyl-bay-substituted perylenediimide core in the dyad and triad (Figures S28-S29).

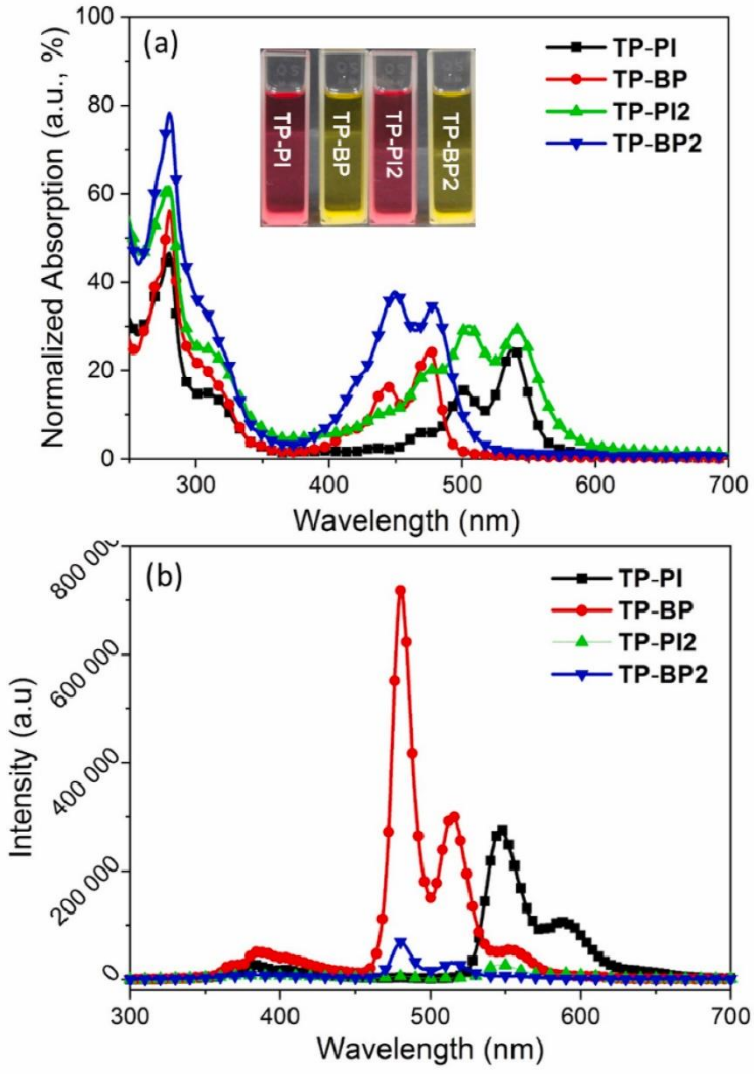

Figure 3. (a) Superimposed UV/vis absorption spectra for the 4 dyads/triads (solution concentrations 10^{-6} M, solvent: CH_2Cl_2). (b) Fluorescence spectra of the dyads and triads. (Concentration: 1×10^{-6} M, non-normalized intensity, excitation 280 nm, CH_2Cl_2). See also Figures S26–S27.

The fluorescence of the dyads (Figure 3b) displayed some degree of acceptor-rylenediimide emission when exciting the donor **TP** unit at 280 nm, due to the intramolecular Forster resonance energy transfer (FRET) from donor-**TP**'s emission to excitation of acceptor. The triads exhibited no or much weaker fluorescence (Figure 3b), which can be explained by stronger intramolecular Dexter charge/electron transfer (ICT) caused fluorescence quenching [23d].

For better understanding the dominating factor of intramolecular electronic energy and electron transfer of these long spacer-connected dyads and triads, we did comparative study of the fluorescence (Figure 4). The dyads and triads showed very weak fluorescence compared to the emission of reference compounds **TP-1**, **PI** and **BP**, implying that the intramolecular charge transfer is the dominant process over the energy transfer. However, when enlarging and careful analysis of the fluorescent spectra, useful information was collected.

Dyads show stronger fluorescence than triads, and the quenching effect is opposite. This effect could be due to the fact that the A-D-A triads **TP**-**PI2** and **TP**-**BP2** possess two accepting moieties per molecule, showing weaker energy transfer-induced fluorescence, and therefore higher degree of intramolecular electron transfer compared to dyads **TP**-**PI** and **TP**-**BP**. Further, **PI** core might be a stronger electron acceptor compared to **BP** core, because the intramolecular charge-transfer (ICT) induced emission quenching is more complete for **TP-PI** and **TP-PI2**.

For the fluorescence spectra, **TP**-**BP** and **TP**-**BP2** were excited at 280 nm (**TP** part), the emitting spectra of both compounds peaked at 480 nm (**BP** part), with a very large Stockes shift of 200 nm due to the Forster resonance energy transfer (FRET) mechanism. Both photoluminescent spectra are almost identical and they emit green light (Figure 4). When dyad **TP**-**PI** is excited at the excitation wavelength of **TP**, i.e. 280 nm, the dyad hardly emits, due to stronger electron transfer (ICT) from **TP** core to **PI** core; the residual emission of the **PI** core is due to energy transfer (Figure 4). When the dyad is excited at 488 nm (**PI** part), it emits weakly, due to the electron transfer from donor **TP** to acceptor **PI**, the quenching of the emission dominates. Compared with **TP**-**PI**, **TP**-**BP** possesses stronger energy transfer and weaker electron transfer between **TP** and **BP** cores, i.e. **PI** core is a stronger electron acceptor.

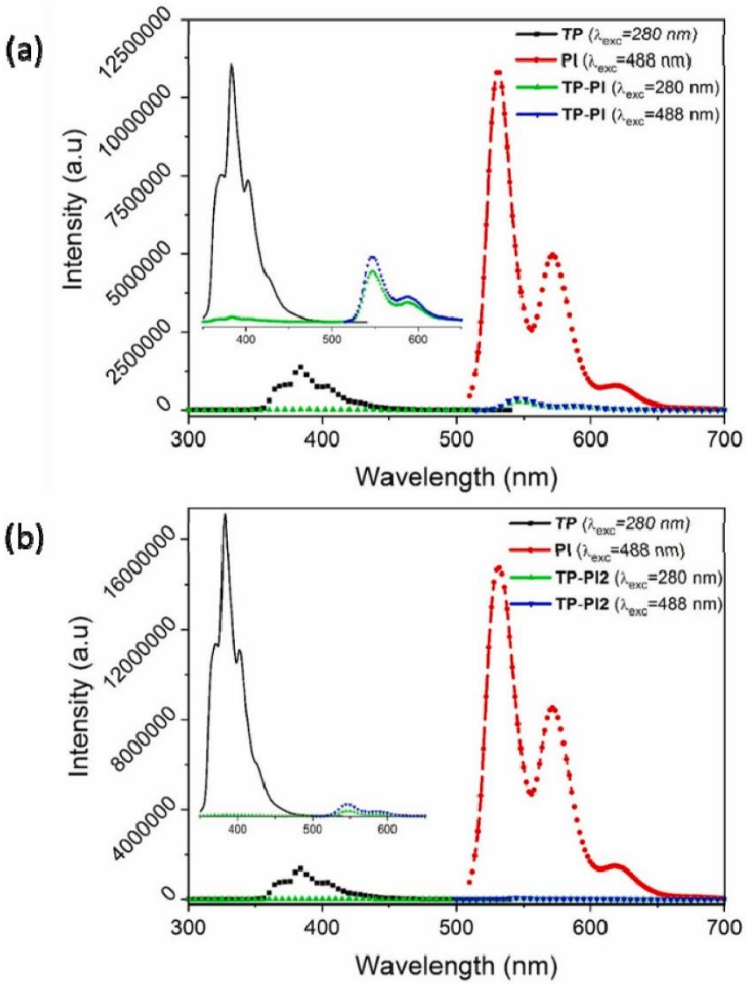

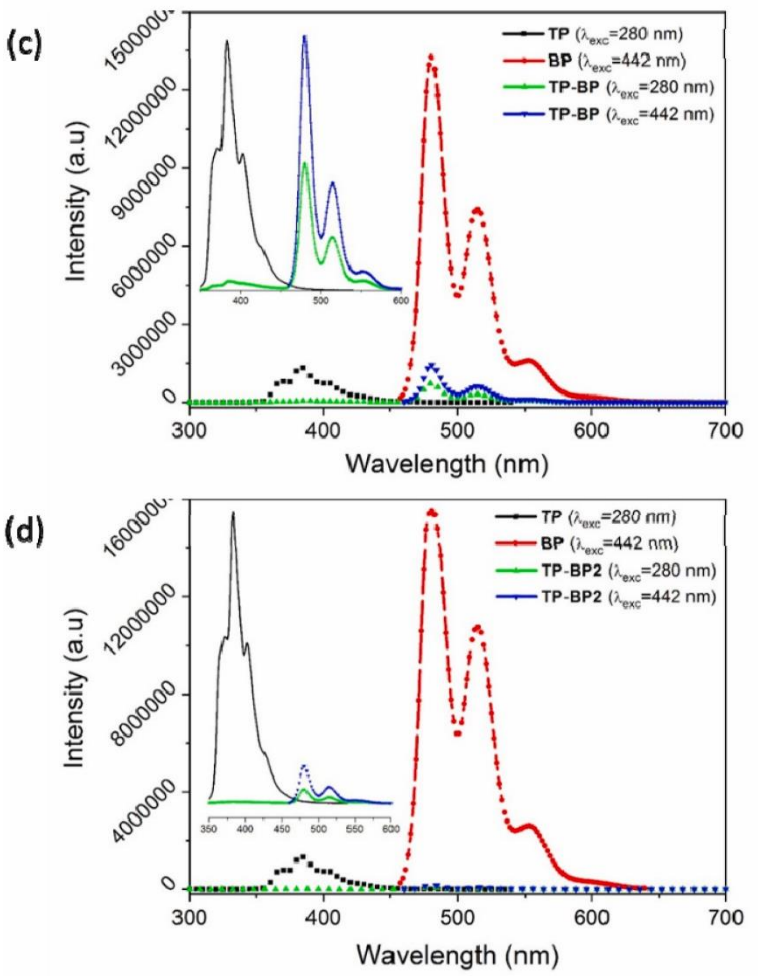

Figure 4. Fluorescence spectra of: (a) **TP**-**PI** (compared with **TP** and **PI**, 10^{-6} M, CH_2Cl_2), (b) **TP**-**PI2** (compared with the reference fluorophores **TP** and **PI**, 10^{-6} M for all, 2. 10^{-6} M for **PI**, CH_2Cl_2), (c) **TP**-**BP** (compared with reference **TP** and **BP**, 10^{-6}M, CH_2Cl_2), and (d) **TP**-**BP2** (compared with the reference fluorophores **TP**, **PI** and **BP**, 10^{-6} M for all, 2.10^{-6} M for **BP**, CH_2Cl_2). As **PI** and **BP** show too strong emission intensity to suppress others, the insert only shows emission of the other fluorophores.

Table 2. Absorption and fluorescence properties of the dyads and triads.

Cpds	λ^a	ε^b	$\lambda_{em}{}^c$	$\lambda_{em}{}^d$	ϕ^d
TP-PI	279	7.81	546 (2.76)	546 (3.56)	16.78
	310	2.51	588 (1.07)	5.88 (1.40)	-
	502	2.62	-	-	-
	538	4.18	-	-	-
TP-BP	280	5.61	480 (7.18)	480 (14.3)	27.6
	307	2.04	515 (2.99)	515 (6.06)	-
	443	1.62	-	-	-
	475	2.45	-	-	-
TP-PI2	279	6.15	546 (0.271)	547 (0.590)	1.35
	310	2.45	587 (0.106)	587 (0.246)	-
	475	2.01	-	-	-
	505	3.00	-	-	-
	540	2.91	-	-	-
TP-BP2	279	7.82	480 (0.697)	481 (1.83)	7.03
	309	3.27	515 (0.306)	515 (0.805)	-

	419	1.69	-	-	-
	449	3.77	-	-	-
	478	3.47	-	-	-

[a]Maximum absorption wavelengths (nm); [b]Extinction coefficient ($\times 10^5$ L mol^{-1} cm^{-1});[c]Emission maxima (nm) with excitation of λ_{ex} = 280 nm and intensity ($\times 10^5$); [d]Emission maxima (nm) with excitation of λ_{ex} = 488 nm and intensity ($\times 10^5$); [d]Fluorescence absolute quantum yield (%) at a concentration of 1×10^{-6} mol L^{-1} in CH_2Cl_2 with excitation on rylenediimide moiety.

When **TP**-**PI2** was excited at the **TP** part or at the **PI** core separately, no emission was detected in any case (ICT). This triad possesses indeed two acceptor **PI** cores, therefore stronger photo-induced electron transfer must occur from the donor to the two acceptors, thus completely quenching the emission. However, weak fluorescent emission is still observed for **TP-BP2** as **BP** core is a weaker electron-acceptor.

The fluorescence quantum yields (φ) of these dyads and triads (Table 2) demonstrate quantitatively the emission efficiency of the rylene diimides, while the parent perylene diimide dyes exhibit φ very close to unity (100%) [24c]. The lowered φ values of these dyads and triads plausibly result from the emission quenching caused by intramolecular charge transfer between donor **TP** and acceptor rylene moieties [23d].

Density functional theory (DFT) was used to study the molecular structures, the HOMO-LUMO energy levels and energy gaps of these dyads and triads (Figure 5, S30-S33), to support the above experimental results. The calculation showed that the molecular structures of the discotic components of the dyads and triads, **TP**, **PI**, and **BP**, are almost planar, which is advantageous for π stacking between the various units to form the discotic columns. The HOMO-1 and HOMO are located on the donor **TP** core, whilst LUMO and LUMO+1 are located on the acceptor cores of **PI** and **BP**; therefore, the photoinduced intramolecular charge-transfer from **TP** to rylenediimide core is highly possible. The calculated LUMO energy levels of **TP**-**PI** and **TP**-**PI2** is lower than that of **TP**-**BP** and **TP**-**BP2**, proving theoretically the stronger electron affinity of **PI** than **BP**, hence the photoinduced electron-transfer of the formers is more complete than the latter, in agreement with the results on photoluminescence.

Finally, DFT calculations show that the HOMO-LUMO energy gaps of the **TP**-**PI** and **TP**-**PI2** (Table S3) are narrower than that of **TP**-**BP** and **TP**-**BP2**, further supporting the experimental results in particular in agreement with the blue-shifted absorption of the benzoperylenediimide (**BP**) compared to alkynyl-perylenediimide (**PI**) core. In summary, photoinduced intramolecular charge transfer (ICT) is the paramount feature for these spacer-connected D-A dyads and A-D-A triads.

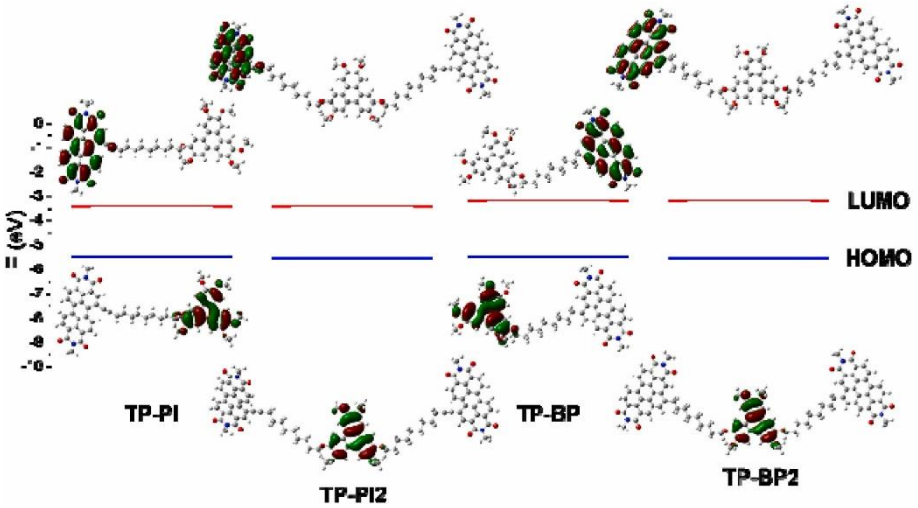

Figure 5. Orbital frontiers, energy levels and gaps for **TP**-**PI**, **TP**-**PI2**, **TP**-**BP**, and **TP**-**BP2** (Calculation method: TD-DFT/b3lyp/6-31 g(d,p), see also Figures S30–S33).

3. Conclusions

Here Four electron-donor/acceptor dyads/triads based on a triphenylene core, as donor (D), and perylene/benzoperylene diimides, as acceptor units (A), both species linked by a long alkyl chain spacer, have been designed and synthesized first by Sonogashira coupling, to bind together **TP** and **PI** species, and then by organic base-promoted intramolecular cyclization to yield the benzoperylenediimide-containing systems, in moderate to good yields. Upon heating, all D-A dyads and A-D-A triads show Col_{hex} or a Col_{rec} mesophase, over broad temperature ranges, including room temperature, with the triads showing higher mesophase stability than the dyads. As demonstrated by S/WAXS, the various molecules unfortunately do not entirely segregate in the volume into perfectly distinct single-compound columns but self-assemble into pseudo-mixed D/A columns instead with some alternation of short-range D- or A-stacks within columns. This intermediate situation is likely due to the conjunction of opposite effects through the chemical connection of different molecular structures but having identical stacking periodicities. The rylenediimide compounds have wide absorption bands but weak emission, due to the intramolecular photo-induced electron transfer between **TP**/**PI** and **TP**/**BP** core. The molecular structures and their HOMO-LUMO energy levels and energy gaps were studied by density functional theory. This analysis is in perfect agreement with the photophysical results and further confirms that **TP** acts as electron-donor system and that the perylenediimide/benzoperylenediimide core are electron-acceptors.

4. Experimental section

All solvents and commercial reagents were used without further purification. The synthesis of the precursors (**PI**, **PI**-**Br**, **TP**-**1**, and **TP**-**2**, Schemes S1–S3) and characterization (NMR, Figures S1–S19, HRMS, Figures S20–S23) are shown in the supplementary information.

Synthesis of TP-PI To a mixture of **PI-Br** (442 mg, 0.48 mmol), CuI (2.7 mg, 0.016 mmol), $Pd(PPh_3)_2Cl_2$ (33.4 mg, 0.048 mmol) and PPh_3 (50.6 mg, 0.098 mmol) in dry toluene (8 mL), a solution of **TP-1** (600 mg, 0.58 mmol) in triethylamine (4 mL) was added under a flux of Ar. The mixture was stirred at 80 °C for 24 h. After reaction completion, the organic phase was extracted with CH_2Cl_2, washed with water, and dried over anhydrous $MgSO_4$. The product was purified by column chromatography (SiO_2, CH_2Cl_2) and crystallized from ethyl acetate-ethanol, yielding a red solid: 0.45 g, 50%. ^{1}H NMR ($CDCl_3$, TMS, 600 MHz), *δ*(ppm): 10.16 (d, *J* = 8.1 Hz, 1H), 8.58 (s, 1H), 8.52 (d, *J* = 8.2 Hz, 1H), 8.40 (d, *J* = 7.9 Hz, 1H), 8.34 (d, *J* = 7.9 Hz, 1H), 8.08 (dd, *J* = 8.0, 2.7 Hz, 2H), 7.55 (d, *J* = 3.6 Hz, 2H), 7.41 (s, 1H), 7.35 (s, 1H), 7.25 (s, 1H), 7.23 (s, 1H), 4.21 (t, *J* = 6.5 Hz, 2H), 4.18 (t, *J* = 6.5 Hz, 2H), 4.13 (d, *J* = 7.3 Hz, 2H), 4.10 (d, *J* = 7.3 Hz, 2H), 4.06 (t, *J* = 6.6 Hz, 2H), 4.00 (t, *J* = 6.6 Hz, 6H), 2.74 (t, *J* = 6.6 Hz, 2H), 2.02–1.80 (m, 16H), 1.72 (dt, *J* = 14.6, 7.3 Hz, 2H), 1.62–1.50 (m, 20H), 1.47–1.22 (m, 86H), 0.92–0.89 (m, 15H), 0.83 (t, *J* = 6.8 Hz, 12H). ^{13}C NMR (151 MHz, $CDCl_3$), *δ*(ppm): 163.73, 163.52, 163.46, 162.99, 148.69, 148.65, 148.50, 148.42, 148.40, 148.36, 138.51, 134.15, 133.59, 133.39, 133.24, 130.54, 130.29, 130.08, 128.41, 127.52, 126.53, 125.99, 125.84, 123.16, 123.09, 122.96, 122.89, 122.84, 122.77, 122.59, 122.57, 122.38, 122.04, 121.64, 120.45, 106.73, 106.67, 106.59, 106.27, 106.04, 105.96, 102.76, 83.00, 69.54, 69.52, 69.37, 69.21, 69.09, 69.04, 44.58, 36.65, 36.62, 31.89, 31.73, 31.69, 30.11, 30.09, 29.79, 29.78, 29.61, 29.58, 29.55, 29.51, 29.38, 29.33, 29.13, 29.04, 28.68, 28.59, 28.02, 26.51, 26.48, 26.29, 26.26, 26.20, 25.89, 22.71, 22.65, 20.30, 14.13. Elemental Analysis Calcd for $C_{125}H_{182}N_2O_{10}$ (MW 1872.835): C, 80.17; H, 9.80; N, 1.50; Found: C, 79.90; H, 9.66; N, 1.71. HRMS (ESI) calcd for $[M]^+$ *m*/*z*: 1872.3828 (100%); Found: 1872.3823.

Synthesis of TP-PI2 **TP-PI2** was synthesized and purified as **TP-PI**. **PI-Br** (1.16 g, 1.2 mmol), **TP-2** (0.34 g, 0.16 mmol), red solid, 0.48 g, 55%. ^{1}H NMR ($CDCl_3$, TMS, 600 MHz), *δ*(ppm): 9.92 (d, *J* = 8.1 Hz, 2H), 8.35 (s, 2H), 8.30 (d, *J* = 8.1 Hz, 2H), 8.21 (d, *J* = 7.8 Hz, 2H), 8.14 (d, *J* = 7.8 Hz, 2H), 7.84 (dd, *J* = 6.9, 1.1 Hz, 1H), 7.10 (s, 2H), 6.98 (s, 2H), 6.82 (s, 2H), 4.08 (d, *J* = 7.1 Hz, 4H), 4.04 (d, *J* = 7.1 Hz, 4H), 4.01 (t, *J* = 6.7 Hz, 4H), 3.97 (t, *J* = 6.5 Hz, 4H), 3.76 (t, *J* = 6.4 Hz, 4H), 2.75 (t, *J* = 6.5 Hz, 4H), 1.99–1.83 (m, 16H), 1.79–1.53 (m, 30H), 1.49–1.22 (m, 130H), 0.94–0.91 (m, 12H), 0.86–0.83 (m, 24H). ^{13}C NMR (151 MHz, $CDCl_3$) *δ*(ppm): 163.48, 163.26, 163.23, 162.73, 148.21, 148.12, 147.96, 138.27, 133.71, 133.20, 132.94, 132.75, 130.20, 129.96, 129.79, 128.17, 127.29, 126.14, 125.58, 125.53, 122.64, 122.51, 122.44, 122.40, 122.36, 122.34, 122.22, 121.82, 121.45, 120.24, 105.70, 105.55, 105.48, 103.18, 69.08, 68.84, 68.82, 44.55, 44.53, 36.70, 36.67, 31.91, 31.70, 31.67, 30.17, 30.14, 29.84, 29.83, 29.66, 29.54, 29.52, 29.42, 29.39, 29.36, 29.18, 28.97, 28.68, 28.65, 28.63, 28.02, 26.48, 26.45, 26.25, 26.24, 25.90, 22.73, 22.68, 22.66, 20.31, 14.15, 14.14, 14.10. Elemental Analysis Calcd for $C_{184}H_{256}N_4O_{14}$ (MW 2748.086): C, 80.42; H, 9.39; N, 2.04; Found: C, 79.90; H, 9.37; N, 2.17. HRMS (ESI) calcd for $[M]^+$ *m*/*z*: 2747.9555 (100%); Found: 2747.9538.

Synthesis of TP-BP A solution of **TP-PI** (0.2 g, 0.11 mmol) and DBU (20 mg) in toluene (5 mL) was stirred and heated at 80 °C under Ar for 24 h. After cooling, the reaction mixture was poured into 2 N HCl and extracted with CH_2Cl_2. After removal of the solvents under reduced pressure, the crude product was purified by a column

chromatography on silica gel (CH_2Cl_2). The product was crystallized from ethyl acetate-ethanol, affording a yellow solid: 0.14 g, 70%. ^{1}H NMR ($CDCl_3$, TMS, 600 MHz), *δ*(ppm): 9.24 (s, 1H), 8.95 (s, 1H), 8.69 (s, 4H), 8.21 (s, 1H), 7.46–7.40 (m, 6H), 4.23 (d, *J* = 7.2 Hz, 4H), 4.13–4.03 (m, 12H), 3.44 (t, *J* = 7.7 Hz, 2H), 2.09–1.85 (m, 16H), 1.66–1.20 (m, 108H), 0.92–0.80 (m, 27H). ^{13}C NMR (151 MHz, $CDCl_3$) *δ*(ppm): 163.99, 163.95, 163.90, 163.82, 148.57, 148.50, 141.28, 133.07, 132.28, 131.74, 129.35, 128.50, 128.23, 127.91, 127.62, 125.99, 125.97, 124.26, 123.03, 123.01, 122.99, 122.97, 122.93, 122.61, 122.45, 122.28, 122.02, 121.99, 121.83, 121.46, 121.29, 106.66, 106.63, 106.56, 106.45, 69.45, 69.39, 69.32, 69.30, 44.84, 44.73, 36.88, 36.80, 33.32, 31.91, 31.89, 31.88, 31.84, 31.81, 31.78, 31.75, 31.16, 30.18, 29.86, 29.65, 29.57, 29.53, 29.51, 29.48, 29.45, 29.35, 29.26, 29.18, 29.05, 26.60, 26.55, 26.51, 26.24, 26.21, 25.96, 22.70, 22.64, 14.11, 14.10, 14.07. Elemental Analysis Calcd for $C_{125}H_{182}N_2O_{10}$ (MW 1872.835): C, 80.17; H 9.80; N 1.50; Found: C, 79.99; H, 9.95; N, 1.48. HRMS (ESI) calcd for $[M]^+$ *m*/*z*: 1872.3828 (100%); Found: 1872.3827.

Synthesis of TP-BP2 **TP**-**BP2** was synthesized and purified as **TP**-**BP**. **PI**-**TP2** (0.2 g, 0.073 mmol), DBU (20 mg), yellow solid, 0.1 g, 55%. ^{1}H NMR ($CDCl_3$, TMS, 600 MHz), *δ*(ppm): 9.10 (s, 2H), 8.75 (s, 2H), 8.42 (d, *J* = 7.1 Hz, 4H), 8.30 (d, *J* = 7.1 Hz, 4H), 8.13 (s, 2H), 6.96 (s, 2H), 6.85 (s, 2H), 6.71 (s, 2H), 4.16 (s, 8H), 4.00 (t, *J* = 5.8 Hz, 4H), 3.83 (t, *J* = 5.3 Hz, 4H), 3.71 (s, 4H), 3.41 (t, *J* = 7.1 Hz, 4H), 2.09–1.22 (m, 176H), 0.92–0.81 (m, 36H). ^{13}C NMR (151 MHz, $CDCl_3$) *δ*(ppm): 163.88, 163.77, 163.69, 163.63, 148.13, 148.03, 148.01, 141.16, 132.83, 131.86, 131.32, 129.23, 129.15, 128.46, 128.13, 127.53, 127.52, 127.28, 125.74, 123.99, 122.70, 122.29, 122.26, 122.18, 122.11, 121.75, 121.62, 121.60, 121.23, 121.10, 106.03, 105.62, 105.39, 68.94, 68.83, 44.81, 44.69, 36.93, 36.84, 33.13, 31.95, 31.92, 31.88, 31.80, 31.79, 31.76, 31.73, 30.75, 30.24, 29.91, 29.70, 29.61, 29.55, 29.46, 29.40, 29.37, 29.24, 28.95, 28.94, 28.78, 28.52, 26.60, 26.54, 26.50, 26.22, 26.21, 25.74, 22.72, 22.71, 22.66, 14.14, 14.12, 14.09. Elemental Analysis Calcd. for $C_{184}H_{256}N_4O_{14}$ (MW 2748.086): C, 80.42; H, 9.39; N, 2.04; Found: C, 80.40; H, 9.49; N, 2.02. HRMS (ESI) calcd for $[M]^+$ *m*/*z*: 2747.9555 (100%); Found: 2747.9510.

Supplementary data

Supplementary data to this article accessible at: https://ars.els-cdn.com/content/image/1-s2.0-S0143720821007774-mmc1.doc

Acknowledgements

This work was financially supported by the National Natural Science Foundation of China (Contract Nos. 21772135, 51773140, and 51973143). BD and BH thank the CNRS and the University of Strasbourg.

References

1 (a) Schmidt-Mende L, Fechtenkotter A, Müllen K, Moons E, Friend RH, MacKenzie JD. Self-organized discotic liquid crystals for high-efficiency organic photovoltaics. Science 2001;293:1119-1122. (b) Bushby RJ, Kelly SM, O'Neill M Eds. Liquid crystalline

semiconductors: Materials, properties and applications. Springer Netherlands, 2013. (c) Ostroverkhova O. Organic Optoelectronic Materials: Mechanisms and Applications. Chem Rev 2016;116:13279-13412.

2 Jiang H. Organic ambipolar conjugated molecules for electronics: synthesis and structure–property relationships, Macromolecular Rapid Commun 2010;31:2007-2034.

3 Gunes S, Neugebauer H, Sariciftci NS. Conjugated polymer-based organic solar cells. Chem Rev 2007;107:1324-1338.

4 Wang MF, Wudl F. Top-down meets bottom-up: organized donor–acceptor heterojunctions for organic solar cells. J Mater Chem 2012;22: 24297–24314.

5 Dong L, Li W, Li WS. Construction of a long range p/n heterojunction with a pair of nanometre-wide continuous D/A phases. Nanoscale 2011;3:3447–3461.

6 Hayashi H, Nihashi W, Umeyama T, Matano Y, Seki S, Shimizu Y, Imahori H. Segregated donor–acceptor columns in liquid crystals that exhibit highly efficient ambipolar charge transport. J Am Chem Soc 2011;133:10736–10739. Addition and correction: J Am Chem Soc 2017;139(39):13957.

7 Adam D, Schuhmacher P, Simmerer J, Haussling L, Siemensmeyer K, Etzbach KH, Ringsdorf H, Haarer D. Fast photoconduction in the highly ordered columnar phase of a discotic liquid crystal. Nature 1994;371:141–143.

8 Wöhrle T, Wurzbach I, Kirres J, Kostidou A, Kapernaum N, Litterscheidt J, Haenle JC, Staffeld P, Baro A, Giesselmann F, Laschat S. Discotic liquid crystals. Chem Rev 2016;116:1139-1241.

9 (a) Sergeyev S, Pisula W, Geerts YH. Discotic liquid crystals: a new generation of organic semiconductors. Chem Soc Rev 2007;36:1902–1929. (b) Kaafarani BR. Discotic liquid crystals for opto-electronic applications. Chem Mater 2011;23:378–396.

10 (a) Irla SK, Mahesh P, Raghunathan VA, Kumar S. Design and synthesis of extended pyrene based discotic liquid crystalline dyes. Dyes Pigm 2021;194:109574. (b) Wang R, Chen S, Chen Q, Guo H, Yang F. Porphyrin with circularly polarized luminescence in aggregated states. Dyes Pigm 2021;190:109332.

11 Zhao KQ, Chen C, Monobe H, Hu P, Wang BQ, Shimizu Y. Three-chain truxene discotic liquid crystal showing high charged carrier mobility. Chem Comm 2011;47:6290-6292.

12 Hang JF, Lin H, Zhao KQ, Hu P, Wang BQ, Monobe H, Zhu C, Donnio B. Butterfly mesogens based on carbazole, fluorene or fluorenone: mesomorphous, gelling, photophysical, and photoconductive properties, Eur. J. Org. Chem 2021;2021:1989-2002.

13 Ma T, Zhong YJ, Wang HF, Zhao KQ, Wang BQ, Hu P, Monobe H, Donnio B. Butterfly-like shape liquid crystals based fused-thiophene as unidimensional ambipolar organic semiconductors with high mobility. Chem Asian J 2021;16:1106-1117.

14 Liu CX, Wang H, Du JQ, Zhao KQ, Hu P, Wang BQ, Monobe H, Heinrich B, Donnio B. Molecular design of benzothienobenzothiophene cored columnar mesogens: facile synthesis, mesomorphism, and charge carrier mobility. J Mater Chem C 2018;6:4471-4478.

15 Zhao KC, Du JQ, Wang HF, Zhao KQ, Hu P, Wang BQ, Monobe H, Heinrich B, Donnio B. Board-like fused-thiophene liquid crystals and their benzene analogs: facile synthesis, self-assembly, p-type semiconductivity, and photoluminescence. Chem Asian J 2019;14:462-470.

16 Shimizu Y, Oikawa K, Nakayama K, Guillon D. Mesophase semiconductors in field effect transistors. J Mater Chem 2007;17:4223–4229.

17 Bala I, Yang WY, Gupta SP, De J, Yadav RAK, Singh DP, Dubey DK, Jou JH, Douali R, Pal SK. Room temperature discotic liquid crystalline triphenylene-pentaalkynylbenzene dyads as an emitter in blue OLEDs and their charge transfer

complexes with ambipolar charge transport behaviour. J Mater Chem C 2019;7:5724-5738.

18 Hassheider T, Benning SA, Kitzerow H, Achard M, Bock H, Color-tuned electroluminescence from columnar liquid crystalline alkyl arenecarboxylates. Angew Chem Int Ed 2001;40:2060–2063.

19 Freudenmann R, Behnisch B, Hanack M. Synthesis of conjugated-bridged triphenylenes and applications in OLEDS. J Mater Chem 2001;11:1618–1624.

20 Kumar S. Recent developments in the chemistry of triphenylene-based discotic liquid crystals. Liq Cryst 2004;31:1037-1059.

21 (a) Kirres J, Schmitt K, Wurzbach I, Giesselmann F, Ludwigs S, Ringenberg M, Ruff A, Baro A, Laschat S, Tuning liquid crystalline phase behaviour in columnar crown ethers by sulfur substituents. Org Chem Front 2017;4:790-803. (b) Feringán B, Romero P, Serrano JL, Folcia CL, Etxebarria J, Ortega J, Termine R, Golemme A, Giménez R, Sierra T. H-bonded donor–acceptor units segregated in coaxial columnar assemblies: toward high mobility ambipolar organic semiconductors. J Am Chem Soc 2016;138:12511-12518. (c) Chico R, de Domingo E, Domínguez C, Donnio B, Heinrich B, Termine R, Golemme A, Coco S, Espinet P. High one-dimensional charge mobility in semiconducting columnar mesophases of isocyano-triphenylene metal complexes. Chem Mater 2017;29:7587−7595. (d) Staffeld P, Kaller M, Beardsworth SJ, Tremel K, Ludwigs S, Laschat S, Giesselmann F. Design of conductive crown ether based columnar liquid crystals: impact of molecular flexibility and geometry. J Mater Chem C 2013;1:892-901.

22 Zhao KQ, Du JQ, Long XH, Jing M, Wang BQ, Hu P, Monobe H, Henrich B, Donnio B. Design of Janus triphenylene mesogens: Facile synthesis, mesomorphism, photoluminescence, and semiconductivity. Dyes Pigm 2017;143:252-260.

23 (a) Nowak-Krol A, Wurthner F. Progress in the synthesis of perylene bisimide dyes. Org Chem Front 2019;6:1272-1318. (b) Markiewicz JT, Wudl F. Perylene, oligorylenes, and aza-Analogs. ACS Appl Mater Interfaces 2015;7:28063−28085. (c) Wurthner F. Perylene bisimide dyes as versatile building blocks for functional supramolecular architectures. Chem Commun 2004;1564–1579. (d) Spenst P, Würthner F. A perylene bisimide cyclophane as a “turn-on” and “turn-off” fluorescence probe. Angew Chem Int Ed. 2015;54:10165–10168. Angew Chem. 2015;127:10303–10306.

24 (a) Weil T, Vosch T, Hofkens J, Peneva K, Müllen K. The rylene colorant family--tailored nanoemitters for photonics research and applications. Angew Chem Int Ed 2010;49:9068-9093. (b) Chen L, Li C, Müllen K. Beyond perylene diimides: synthesis, assembly and function of higher rylene chromophores. J Mater Chem C 2014;2:1938-1956. (c) Wurthner F, Saha-Moller CR, Fimmel B, Ogi S, Leowanawat P, Schmidt D. Perylene bisimide dye assemblies as archetype functional supramolecular materials. Chem Rev 2016;116:962-1052. (d) Zhang G, Zhao J, Chow PCY, Jiang K, Zhang J, Zhu Z, Zhang J, Huang F, Yan H. Nonfullerene acceptor molecules for bulk heterojunction organic solar cells. Chem Rev, 2018;118:3447-3507.

25 Struijk CW, Sieval AB, Dakhorst JEJ, Dijk MV, Kimkes P, Koehorst RBM, Donker H, Schaafsma TJ, Picken SJ, Van de Craats AM, Warman JM, Zuilhof H, Sudhölter EJR. Liquid crystalline perylene diimides: architecture and charge carrier mobilities. J Am Chem Soc 2000;122:11057–11066.

26 (a) Wicklein A, Lang A, Much M, Thelakkat M. Swallow-tail substituted liquid crystalline perylene bisimides: synthesis and thermotropic properties. J Am Chem Soc 2009;131:14442–14453. (b) Pu J, Yang T, Wang Y, Zhu Q, Yang M, Liu C, Wang W. Tunable self-organization in n-type liquid crystalline dibenzocoronene tetracarboxdiimides for high photoconductivity. Liq Cryst 2020;47:291-300.

27 Gupta RK, Sudhakar AA. Perylene-based liquid crystals as materials for organic electronics applications. Langmuir 2019;35:2455-2479.

28 Kong X, He Z, Zhang Y, Mu L, Liang C, Chen B, Jing X, Cammidge AN. A mesogenic triphenylene−perylene−triphenylene triad. Org Lett 2011;13:764-767.

29 Gupta SK, Setia S, Sidiq S, Gupta M, Kumar S, Pal SK. New perylene-based non-conventional discotic liquid crystals. RSC Adv 2013;3:12060-12065.

30 Xiao Y, Su X, Sosa-Vargas L, Lacaze E, Heinrich B, Donnio B, Kreher D, Mathevet F, Attias AJ. Chemical engineering of donor–acceptor liquid crystalline dyads and triads for the controlled nanostructuration of organic semiconductors. CrystEngComm 2016;18:4787-4798.

31 Guo H, Zhu M, Wang Z, Yang F. Triphenylene–perylene–triphenylene triads with bay-substituents: synthesis, mesomorphism, and electron transfer properties. Tet Lett 2016;57:4191-4195.

32 Lee KJ, Woo JH, Kim E, Xiao Y, Su X, Mazur LM, Attias AJ, Fages F, Cregut O, Barsella A, Mathevet F, Mager L, Wu JW, D'Aléo A, Ribierre JC. Electronic energy and electron transfer processes in photoexcited donor–acceptor dyad and triad molecular systems based on triphenylene and perylene diimide units. Phys Chem Chem Phys 2016;18:7875-7887.

33 Kong X, Xia L, Zhang H, Dai S, Yu C, Liu Z, Mu L, Wang G, He Z. Synthesis and investigation on liquid crystal and optical properties of dyads based on triphenylene and perylene. RSC Adv 2017;7:17030-17037.

34 Kong X, Gong H, Liu P, Yao W, Liu Z, Wang G, Zhang S, He Z. Synthesis and investigation on optoelectronic properties of mesogenic triphenylene–perylene dyads linked by ethynylphenyl bridges. New J Chem 2018;42:3211-3221.

35 Zhao KQ, An LL, Zhang XB, Yu WH, Hu P, Wang BQ, Xu J, Zeng QD, Monobe H, Shimizu Y, Heinrich B, Donnio B. Highly segregated lamello-columnar mesophase organizations and fast charge carrier mobility in new discotic donor–acceptor triads. Chem Eur J 2015;21:10379-10390.

36 Zhao KQ, Gao Y, Yu WH, Hu P, Wang BQ, Heinrich B, Donnio B. Discogens possessing aryl side groups synthesized by suzuki coupling of triphenylene triflates and their self-organization behavior. Eur J Org Chem 2016;2016:2802-2814.

37 (a) Das A, Ghosh S. A generalized supramolecular strategy for self-sorted assembly between donor and acceptor gelators. Chem Commun 2011;47:8922-8924. (b) Das A, Molla MR, Maity B, Koley D, Ghosh S. Hydrogen-bonding induced alternate stacking of donor (D) and acceptor (A) chromophores and their supramolecular switching to segregated states. Chem. Eur J 2012;18:9849–9859. (c) Kobaisi MA, Bhosale RS, El-Khouly ME, La DD, Padghan SD, Bhosale SV, Jones LA, Antolasic F, Fukuzumi S, Bhosale SV. The sensitivity of donor – acceptor charge transfer to molecular geometry in DAN – NDI based supramolecular flower-like self-assemblies. Sci Rep 2017;7:16501. (d) Gabriel GJ, Sorey S, Iverson BL. Altering the folding patterns of naphthyl trimers. J Am Chem Soc 2005;127:8, 2637–2640.

38 (a) Zucchi G, Viville P, Donnio B, Vlad A, Melinte S, Mondeshki M, Graf R, Spiess HW, Geerts YH, Lazzaroni R. Miscibility between differently shaped mesogens: Structural and morphological study of a phthalocyanine-perylene binary system. J Phys Chem B 2009;113:5448-5457. (b) Zhong T, Mandle R, Saez I, Cowling S, Goodby JW. Rods to discs in the study of mesomorphism in discotic liquid crystals. Liq Cryst 2018;45:2274-2293. (c) Kreouzis T, Donovan KJ, Boden N, Bushby RJ, Lozman OR, Liu Q. Temperature-independent hole mobility in discotic liquid crystals. J Chem Phys 2001;114:1797-1802.

39 Myśliwiec D, Donnio B, Chmielewski PJ, Heinrich B, Stępień M. Peripherally fused porphyrins via the Scholl reaction: synthesis, self-assembly, and mesomorphism. J Am Chem Soc 2012;134:4822-4833.

40 Dössel LF, Kamm V, Howard IA, Laquai F, Pisula W, Feng X, Li C, Takase M, Kudernac T, De Feyter S, Müllen K. Synthesis and controlled self-assembly of covalently linked

hexa-peri-hexabenzocoronene/perylene diimide dyads as models to study fundamental energy and electron transfer processes. J Am Chem Soc 2012;134:5876-5886.

41 Lee KJ, Xiao Y, Woo JH, Kim E, Kreher D, Attias AJ, Mathevet F, Ribierre JC, Wu JW, Andre P. Charge-transfer dynamics and nonlocal dielectric permittivity tuned with metamaterial structures as solvent analogues, Nature Mater 2017;16:722-729.

42 Kong X, Liu P, Wang G, Xia L, Dai S, Su J, Liao P, Liu Z, Mu L. Synthesis and investigation on liquid crystal and optical properties of dyads based on triphenylene and perylene. Chin J Org Chem 2016;36:1325-1334.

43 Hecht M, Schlossarek T, Ghosh S, Tsutsui Y, Schmiedel A, Holzapfel M, Stolte M, Lambert C, Seki S, Lehmann M, Würthner F. Nanoscale columnar bundles based on multistranded core–shell liquid crystals of perylene bisimide J-aggregate donor–acceptor dyads for photoconductivity devices with enhanced performance through macroscopic alignment. ACS Appl Nano Mater 2020;3:10234-10245.